Pb(II) biosorption on Posidonia oceanica biomass

Fella-Naouel Allouche, Nabil Mameri, Guibal Eric

Pb(II) biosorption on *Posidonia oceanica* biomass

Fella-Naouel Allouche[a,b,c], Nabil Mameri[d], Eric Guibal[a,*]

[a] *Ecole des Mines d'Alès, Laboratoire Génie de l'Environnement Industriel, 6, Avenue de Clavières, F-30319 Alès Cedex, France*
[b] *Centre de Développement des Energies Renouvelables, Laboratoire de Bioénergie et Environnement, B.P. 62, Route de l'Observatoire, Bouzaréah-Alger, Algeria*
[c] *Ecole Nationale Supérieure Agronomique, 12, Hacen Badi, El Harrach-Alger, Algeria*
[d] *Ecole Nationale Polytechnique d'Alger, Laboratoire des Biotechnologies Environnementales et Génie des Procédés, 10, Hacen Badi, El Harrach-Alger, Algeria*

A B S T R A C T

Posidonia oceanica leaves have been pre-treated with HCl solutions to elaborate a biosorbent that was carried out for Pb(II) sorption at pH 4 and pH 5. The sorption of Pb(II) was characterized using SEM-EDAX, XPS spectrometry and FT-IR spectroscopy. Maximum sorption capacity reached up to 140 mg Pb g^{-1} at pH 5. The uptake kinetics were controlled by chemisorption reaction rate. This was correlated to the lamellar structure observed using SEM analysis. The influence of sorbent dosage, particle size and metal concentration on uptake kinetics was also investigated. Sorption performances are compared to other biosorbents and to previous studies on *P. oceanica* for binding of mineral and organic compounds.

Keywords:
Pb(II)
Posidonia oceanica
Biosorption
SEM
SEM-EDAX
Sorption isotherm
Uptake kinetics
XPS
pH effect

1. Introduction

All over the world the environmental regulations are becoming progressively more stringent regarding the dispersion of contaminants in nature. Nowadays, the discharge of wastewaters to the environment is more and more controlled. Among the target contaminants, heavy metals have retained a great attention since they can have a direct health impact through absorption and because they can be bioaccumulated. The accumulation in soil, sediments, in the food chain can cause *in fine* dramatic effects on human health: the case of Minamata in Japan with mercury accumulation in the food chain is a perfect example of the potential hazards of metal dispersion. Lead is one of the most controlled metal in wastewaters: its maximum admissible concentration in drinking water was fixed to 10 $\mu g\,L^{-1}$ by European Union [1].

A number of processes have been designed for metal recovery from industrial effluents including precipitation [2], solvent extraction [3,4], resins [5–8], solvent impregnated materials [9], membrane processes [10,11]. These conventional processes are frequently inappropriate, especially for low-concentration solutions due to economic, technical or environmental reasons. The processes are not competitive when metal concentration is below 50–100 mg L^{-1}; they may face limitations for reaching target concentrations, or they may have direct or indirect impact on environment. For example, in the case of synthetic resins, the products may be difficult to eliminate at the end of their life cycle [12]. The selection of the sorbent may thus take into account a number of criteria such as: competitiveness, technical efficiency, environmental impact, life cycle and sustainable growth parameters. Biosorption has been cited as a promising alternative. The concept of biosorption is based on the use of alternative materials: bacteria [13,14], alga [15–17], yeast [18], fungi [19,20], but also sub-products of agriculture [21,22] or industry, biopolymers [23–25]. These renewable resources are characterized by the presence of a number of reactive groups similar to those found on conventional resins and they can be used for metal binding through a number of different reactions including ion exchange, electrostatic attraction, complexation [26]. Additionally, they are less hazardous in terms of elimination at the end of their life cycle (thermal degradation for example) [12].

Marine biomass represents an important resource for biosorption processes. The biomass can be used as raw material (algal biosorbent) or as a precursor for more elaborated biosorbents such as biopolymers (alginate and chitosan). While algal materials have been widely investigated for metal biosorption [27], the potential of marine plants such as *Posidonia oceanica* (Neptune grass) has been notably understudied. This material is very abundant in the Mediterranean sea. *P. oceanica* biomass is a highly fibrous material made of cellulose and hemicellulose (about 60–75%) and lignin

* Corresponding author. Tel.: +33 4 66 78 2734; fax: +33 4 66 78 2701.
E-mail address: Eric.Guibal@mines-ales.fr (E. Guibal).

(about 25–30%) plus a non-negligible percentage of ash that contains essentially silica but also some heavy metals [28]. *P. oceanica* has been used as a marker for metal contamination [29–32]. But the biomass was also tested for the sorption of organic contaminants [33], dyes [34–38], and more recently for inorganic compounds [39–41]. *P. oceanica* biomass was also used for the synthesis of sorbents, which were obtained by reaction with succinic anhydride. The modified sorbent was carried out for the sorption of Pb(II) and direct red 75 dye [42].

Preliminary tests have shown that *P. oceanica* biomass has a marked preference for Pb(II) compared to Cd(II), Ni(II) and Hg(II). This study focuses on the investigation of Pb(II) sorption on HCl pre-treated *P. oceanica* biomass. The treatment of *P. oceanica* with distilled water induces a partial leaching of some elements (including S, Mg, Na, Zn, Pb, Cd, Fe, Cr and Ti, [43]). Additionally, the pre-treatment with acid solutions allows removing/releasing some organic compounds by leaching; these organic compounds may contribute to the partial precipitation of metal ions. In order to improve the stability of the biosorbent (and reduce pH variation during sorption experiments) it appeared necessary applying this acidic pre-treatment. The study successively investigates (a) the effect of pH on metal sorption (for determining optimum operating conditions), (b) the sorption isotherms, and (c) the uptake kinetics. Apart these studies of macroscopic sorption properties, the materials were also characterized by SEM and SEM-EDAX analysis, by FT-IR spectroscopy and XPS spectrometry.

2. Materials and methods

2.1. Biosorbent and materials

Fresh samples of *P. oceanica* (a flowering plant that lives in dense meadows) were harvested from the West coast of Algiers. The leaves are ribbon-like; they are bright green turning brown with age, while rhizome type stems grown in and at the surface of sand. In the present study, the biosorbent was prepared from the leaves. After being collected the samples were rinsed with tap water to remove impurities such as sand and salt absorbed at the surface of the biomass. The biomass was cut in strips of 2–4 cm length. The biomass was treated for 1 h with 0.1 M HCl solution before being rinsed several times till neutral pH. Finally, the biosorbent was dried in an oven at 60 °C for 24 h. Dried material was ground and sieved in different size fractions, which are prioritized from small to large as: G1 (<125 μm), G2 (125–250 μm), G3 (250–500 μm), G4 (500–710 μm), and G5 (710–1000 μm).

Lead stock solutions were prepared by dissolving lead acetate ($Pb(C_2H_3COO)_2{\cdot}3\ H_2O$, Carlo Erba) in acidified water. Solutions were prepared by the dilution of the stock solution in demineralized water (Milli-Q).

2.2. Sorption experiments

The influence of pH was studied by contact of the biosorbent (m: 50 mg, 100 mg, 200 mg or 300 mg of the biosorbent at the particle size G3) with a volume V (L) of 100 mL of the metal solution (initial concentration, C_0: 50 mg Pb L^{-1}) at target pH values. The initial pH was set between 2.0 and 6.0. The pH was controlled using molar solutions of HCl and NaOH. After one day of agitation on a reciprocal shaker (150 movements per min), the solution was filtrated using a 1–2 μm pore size filtration membrane and the filtrate was analyzed by ICP-AES (Jobin-Yvon Activa-M, Jobin-Yvon, Longjumeau, France) for equilibrium metal concentration (C_{eq}: mg metal L^{-1} or mmol metal L^{-1}). The mass balance equation was used for calculating the sorption capacity q (mg metal g^{-1}, or mmol metal g^{-1}), according to: $q = (C_0 - C_{eq})\,V/m$. The final pH was systematically monitored at equilibrium (WTW pH meter, Model 526 pH, with pH electrode ref. SenTix 41, Germany).

Uptake kinetics was determined at room temperature mixing 0.5 L of solution with a fixed amount of sorbent. The suspension was mixed using a magnetic bar and stirrer at the agitation speed of 200 rpm. Samples were collected at different contact times, filtrated and analyzed by ICP-AES for the determination of the kinetic profile (plotting the relative concentration $C(t)/C_0$ versus time). The amount of sorbent (i.e., sorbent dosage, SD, g L^{-1}), the initial metal concentration (C_0, mg L^{-1}) and the particle size (G1–G5) were varied: relevant experimental conditions are extensively described in the caption of the figures.

Sorption isotherms were performed at pH 4 and 5 (optimum pHs) for Pb(II). A given amount of sorbent (i.e., 100 mg of biosorbent, G1–G5) was dropped into 100 mL of metal solution at the appropriate pH. The initial metal concentration was varied between 10 and 200 mg metal L^{-1}. The suspension was maintained under agitation for 24 h using a reciprocal shaker (velocity: 150 movements per min) at room temperature (i.e., 20 ± 1 °C). Finally, the suspension was filtrated and the residual concentration of metal was analyzed by ICP-AES.

2.3. Material characterization

The biomass was analyzed by FT-IR spectroscopy (FT-IR Bruker equipped with OPUS Software) after inclusion in KBr discs. SEM-EDAX analysis was also performed on the biomass for observation and identification of binding localization. The dry sorbent was analyzed using an Environmental Scanning Electron Microscopy (ESEM) Quanta FEG 200, equipped with an OXFORD Inca 350 Energy Dispersive X-ray microanalysis (EDX) system.

The chemical characterisation of the surface of the studied samples was performed by XPS. A Physical Electronics spectrometer (PHI 5700) was used, with X-ray Mg Kα radiation (300 W, 15 kV, 1253.6 eV) as the excitation source. High-resolution spectra were recorded at a given take-off angle of 45° by a concentric hemispherical analyser operating in the constant pass energy mode at 29.35 eV, using a 720 μm diameter analysis area. Under these conditions, the Au $4f_{7/2}$ line was recorded with 1.16 eV FWHM at a binding energy of 84.0 eV. The spectrometer energy scale was calibrated using Cu $2p_{3/2}$, Ag $3d_{5/2}$, and Au $4f_{7/2}$ photoelectron lines at 932.7, 368.3, and 84.0 eV, respectively. Charge referencing was done against adventitious carbon (C 1*s*, 284.8 eV). Samples were mounted on a sample holder without adhesive tape and kept overnight at high vacuum in the preparation chamber before being transferred to the analysis chamber of the spectrometer. Each spectral region was scanned several sweeps up to a good signal to noise ratio was observed. The pressure in the analysis chamber was maintained lower than 5×10^{-6} Pa. PHI ACCESS ESCA-V6.0 F software package was used for acquisition and data analysis. A Shirley-type background was subtracted from the signals. Recorded spectra were always fitted using Gauss–Lorentz curves, in order to determine more accurately the binding energy (BE) of the different element core levels. Atomic concentration percentages of the characteristic elements of the surfaces were determined taking into account the corresponding area sensitivity factor for the different measured spectral regions.

3. Results and discussion

3.1. pH effect on Pb(II) sorption

The pH is an important parameter for biosorption processes since it may affect the speciation of the metal (metal distribution, precipitation, complexation), the stability of the biomass (potential degradation, leaching of some compounds and functional

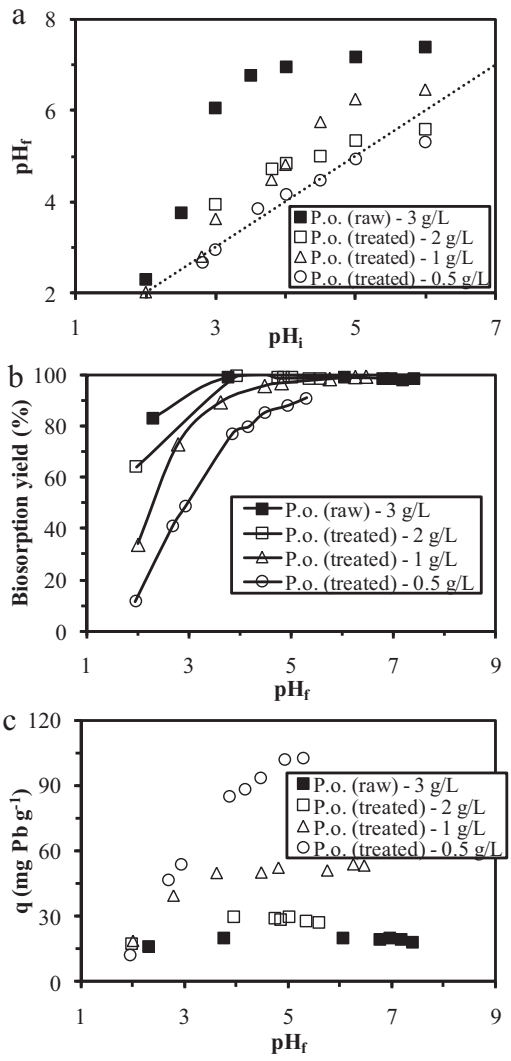

Fig. 1. Influence of pH on Pb(II) sorption using *Posidonia* biosorbent: (a) pH variation during metal sorption; (b) biosorption yield; (c) sorption capacity (V: 100 mL; C_0: 50 mg Pb L^{-1}; Sorbent dosage, SD (g L^{-1}): variable; PS: G3).

groups) and the chemical state of its reactive groups (protonation/deprotonation). Fig. 1 shows the impact of pH on biosorption yield (Fig. 1(b)) and sorption capacity (Fig. 1(c)) but also pH variation during metal sorption (Fig. 1(a)).

The pre-treatment of the biomass with HCl allows reducing the variation of pH during metal sorption. This is important for stabilizing the material, for reducing the possible occurrence of local phenomena of metal micro-precipitation and for comparison of sorption performance. A biosorbent that changes the pH of the solution makes difficult the comparison of sorption performance and the determination of sorption characteristics (for example sorption isotherms). Increasing the amount of sorbent obviously increases the impact on pH variation (Fig. 1(a)). The sorption efficiency increases (Fig. 1(b)) with pH. Similar trends were observed for ammonium binding on *P. oceanica* [39]. Under acidic conditions, the reactive groups are protonated due to the competition effect of protons and these reactive groups are not available for cation binding. Izquierdo et al. [40] investigated copper sorption on *P. oceanica* and they showed that the pH_{ZPC} is close to 8.2. This means that in neutral and acid solutions the biosorbent is positively charged. However, increasing the pH reduces the density of positive charges and the repulsion effect for the binding of metal cations. Hence they observed an increase of Cu(II) sorption capacity from pH 5 to pH 6.

Table 1
Influence of sorbent dosage (SD, g L^{-1}) on Pb(II) uptake kinetics at pH 4—modeling with the PFORE and the PSORE (G4 particle size; [Pb(II)]: 50 mg L^{-1}).

SD	PFORE				PSORE		
	q_{exp}	q_{mod}	k_1	R^2	q_{mod}	$k_2 \times 10^3$	R^2
0.3	104	100.8	0.0382	0.993	110.6	0.44	0.977
0.5	95	95.3	0.053	0.989	102.5	0.72	0.970
0.75	75	74.9	0.060	0.997	80.3	1.05	0.978
1	54	54.5	0.099	0.997	57.1	2.70	0.981
1.25	49	49.3	0.104	0.999	52.0	3.07	0.987

q: mg Pb g^{-1}; k_1: min^{-1}; k_2: g mg^{-1} min^{-1}.

When the pH increases above 8, the fiber biopolymers, mainly lignin and cellulose chains, become negatively charged, which, in turn makes possible the binding of cations through electrostatic attraction mechanism [39]. In the case of ammonium binding, Wahab et al. [39] report several mechanisms: ion exchange mechanism of ammonium cation on –ROH and –RCOOH groups but ammonia hydroxide was also bound through hydrogen bonding on the same functional polar groups. In the case of chromium(VI) biosorption on *P. oceanica* fibers, Ncibi et al. [41] observed a completely different behavior. The sorption capacity decreased with increasing the pH. The deprotonation of reactive groups gives a neutral or anionic surface coverage which is not favorable for the binding of metal anions. Additionally, the pH changes the speciation of Cr(VI) species in the solution and their affinity for the biosorbent. Similar reduction of sorption efficiency was observed on the binding of textile metal-complexed dyes using also *P. oceanica* [34]: the anionic dyes are preferentially adsorbed in acidic conditions corresponding to the protonation of reactive groups at the surface of the biosorbent.

Under selected experimental conditions (i.e., C_0: 50 mg Pb L^{-1}) biosorption yield exceeded 98% when the equilibrium pH reached 5 for a sorbent dosage of 1 g L^{-1}, and pH 4 for a higher sorbent dosage (i.e., 2 or 3 g L^{-1}) (Fig. 1(b)). The sorption capacity logically increases with pH (Fig. 1(c)) and decreases with sorbent dosage: the stabilization of sorption capacity observed on this figure is due to the complete recovery of the metal from the solution and it is not indicative of the maximum sorption capacity of the material for given pH values. For following experiments initial pH 4 and 5 were tested: these values allow combining favorable conditions for equilibrium pH (consistent with metal stability, avoiding precipitation) and high sorption efficiency.

3.2. Uptake kinetics

The effects of sorbent dosage, particle size and metal concentration on uptake kinetics have been carried out and the kinetic profiles were fitted to different models including the pseudo-first order rate equation (PFORE) and the pseudo-second order rate equation (PSORE) (see Additional Material Section). The parameters of the models will be shown in Tables 1–3. Generally the PFORE model allows approaching more accurately experimental data as

Table 2
Influence of particle size (PS) on Pb(II) uptake kinetics at pH 5—modeling with the PFORE and the PSORE (SD: 0.5 g L^{-1}; [Pb(II)]: 50 mg L^{-1}).

PS	PFORE				PSORE		
	q_{exp}	q_{mod}	k_1	R^2	q_{mod}	$k_2 \times 10^3$	R^2
G1	90	89.3	0.268	9.998	92.3	4.5	0.988
G2	106	106.0	0.096	0.999	111.9	1.28	0.983
G3	101	101.1	0.064	0.995	107.8	0.87	0.988
G4	102	101.3	0.052	0.997	109.4	0.67	0.991
G5	102	98.8	0.034	0.989	109.4	0.40	0.974

q: mg Pb g^{-1}; k_1: min^{-1}; k_2: g mg^{-1} min^{-1}.

Table 3
Influence of metal concentration (C_0: mg Pb L^{-1}) on Pb(II) uptake kinetics at pH 4—modeling with the PFORE and PSORE (SD: 0.5 g L^{-1}; PS: G4).

C_0	PFORE				PSORE		
	q_{exp}	q_{mod}	k_1	R^2	q_{mod}	$k_2 \times 10^3$	R^2
20	40	40.8	0.050	0.989	44.0	1.52	0.969
50	95	95.3	0.053	0.989	102.5	0.72	0.970
100	139	140.0	0.071	0.991	149.0	0.69	0.976

q: mg Pb g^{-1}; k_1: min^{-1}; k_2: g mg^{-1} min^{-1}.

shown by the correlation coefficient and also by the comparison of sorption capacities at equilibrium. The differences between experimental values and the modeled values of q_m obtained were, in most cases, less marked for the PFORE model (less than 3%) than for the PSORE model.

3.3. Effect of sorbent dosage (SD)

Fig. 2 shows the effect of sorbent dosage on Pb(II) uptake kinetics at initial pH 4. The final pH, regardless of the SD, was between 4.05 and 4.52: the pH variation increased with sorbent dosage but due to the pre-treatment of the biomass the pH change was limited. A contact time of 2–4 h is generally sufficient for achieving the equilibrium, under selected experimental conditions. Though the modeling of the curves in the curvature zone was not perfect the PSORE allowed roughly describing the kinetic trends. The modeling with the Crank's equation (on plane membrane), which represents the resistance to intraparticle diffusion also failed to fit the curvature zone (not shown). This probably means that several phenomena are involved in the control of mass transfer (including resistance to film diffusion, to intraparticle diffusion and the proper reaction rate). Table 1 summarizes the parameters of the models. The modeled equilibrium sorption capacity (q_{mod}) systematically overestimates the experimental value. Its value logically decreased with increasing sorbent dosage due to the higher rationale use of reactive groups when using lower sorbent dosage (approaching biosorbent saturation). On the opposite hand, when the sorbent dosage increased the kinetic parameter, k_2 (mg g^{-1} min^{-1}), linearly increased from 4×10^{-4} to 3.1×10^{-3} g mg^{-1} min^{-1}, according to:

$$k_2 = 3.04 \times 10^{-3} \times SD - 7.12 \times 10^{-4} \quad (R^2 = 0.918) \qquad (1)$$

where SD is the sorbent dosage (g L^{-1}).

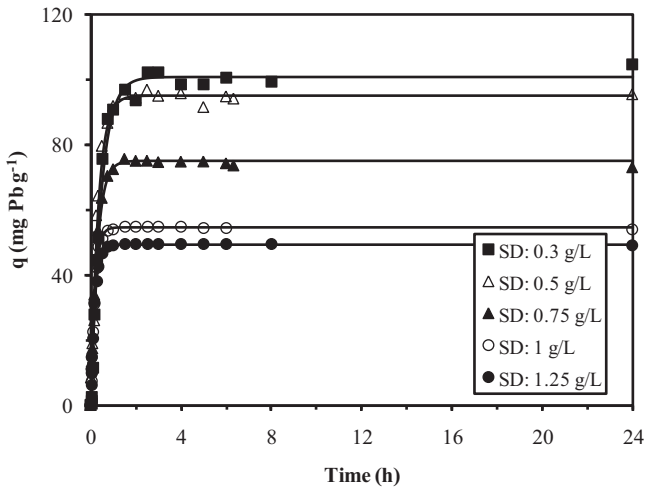

Fig. 2. Influence of sorbent dosage (SD) on Pb(II) uptake kinetics (pH 4; PS: G4, 500–710 μm; C_0: 50 mg Pb L^{-1}: curves represent the modeling of uptake kinetics with the PFORE).

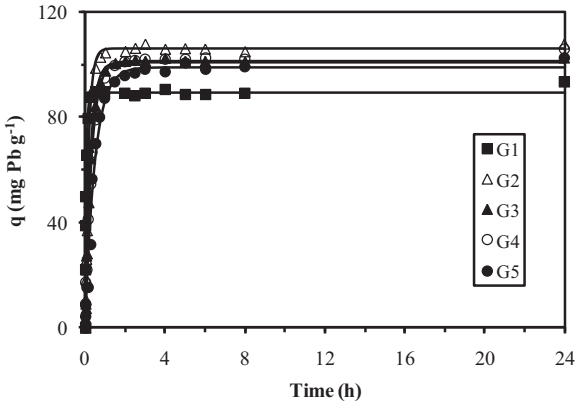

Fig. 3. Influence of particle size (PS, μm: 0 < G1 < 125 < G2 < 250 < G3 < 500 < G4 < 710 < G5 < 1000) on Pb(II) uptake kinetics (pH 5; SD: 0.5 g L^{-1}; C_0: 50 mg Pb L^{-1}: curves represent the modeling of uptake kinetics with the PFORE).

These values are much lower than those cited for dye [44] and for ammonium [39] sorption using *P. oceanica* biosorbent: 0.035–0.377 g mg^{-1} min^{-1} and 0.37–0.57 g mg^{-1} min^{-1}, respectively. But they are slightly higher than those obtained in the case of Pb(II) sorption using a red alga (*Chondracanthus chamissoi*) (i.e., $0.1–0.4 \times 10^{-3}$ g mg^{-1} min^{-1}) [45]. In this case the kinetic parameter slightly increased with SD for Pb(II) sorption while it remained almost constant for Cd(II) uptake.

With the PFORE model, the q_m obtained by the model is much closer to the experimental values than for PSORE model (Table 1). The kinetic parameter k_1 (min^{-1}) linearly increases with SD according to:

$$k_1 = 0.074 \times SD + 0.0145 \quad (R^2 = 0.934) \qquad (2)$$

Chadlia et al. [42] also observed that the PFORE model fitted better experimental data than the PSORE model for the sorption of lead on a chemical derivative of *P. oceanica* obtained by succinic anhydride grafting. The values of the kinetic parameter reported by Chadlia et al. are significantly higher (i.e., between 0.20 and 0.86 min^{-1}) than those obtained in the present study (i.e., 0.04–0.1 min^{-1}).

3.4. Effect of particle size (PS)

The particle size is an important parameter that should be checked to verify the contribution of the resistance to intraparticle diffusion on the control of uptake kinetics. Fig. 3 shows that this parameter had a limited impact on kinetic profiles (experiments carried out at pH 5). The curves almost overlapped indicating that the particle size has a limited impact on mass transfer. This is first evidence that the resistance to intraparticle diffusion is probably not the limiting step in the sorption process. This is consistent with the morphology and the structure of the biosorbent as shown by SEM and SEM-EDAX analyses (see below): the lamellar structure allows metals ions to access internal reactive groups. Ncibi et al. also [41] reported that Cr(VI) sorption on *P. oceanica* is controlled by chemisorption rate rather than mass transfer resistance. The slightly lower performance for G1 particle size may be due to a partial degradation of the biomass during grinding operations [45].

There was no difference for particle sizes G2–G5 (i.e., 125–1000 μm), and a slight decrease of sorption performance for the smallest particles (below 125 μm). This is confirmed by the equilibrium sorption capacity for the PSORE (Table 2): a 10% increase was observed between G1 and G2 fractions followed by a stabilization of the uptake capacity. The kinetic rate (i.e., k_2) decreased with particle size; however, the most sig-

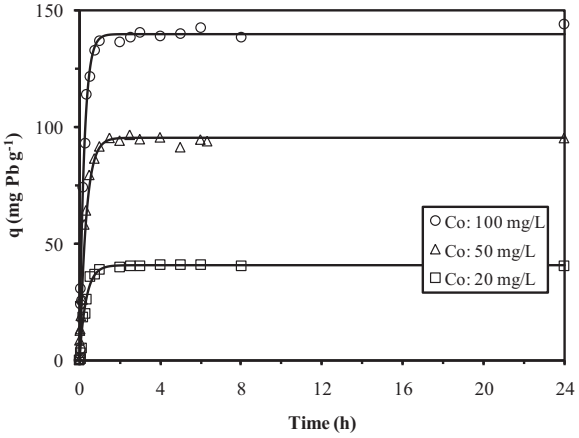

Fig. 4. Influence of initial metal concentration (C_0, mg Pb L^{-1}) on Pb(II) uptake kinetics (pH 4; SD: 0.5 g L^{-1}; C_0: 50 mg Pb L^{-1}; PS: G4; curves represent the modeling of uptake kinetics with the PFORE).

nificant difference was observed between G1 and G2 particle sizes (from 4.5×10^{-3} g mg^{-1} min^{-1} to 1.3×10^{-3} g mg^{-1} min^{-1}), while for largest particles the variation was rather limited (from 1.3×10^{-3} g mg^{-1} min^{-1} to 0.4×10^{-3} g mg^{-1} min^{-1}). Actually, the kinetic parameter k_2 linearly increases with the reciprocal of average diameter of sorbent particles (d, μm) according to:

$$k_2 = 0.272 \times \left(\frac{1}{d}\right) + 8.39 \times 10^{-6} \quad (R^2 = 0.997) \tag{3}$$

It is interesting to compare data obtained at pH 4 (Table 1) with the relevant information obtained at pH 5 (Table 2) for similar sorbent dosage (SD: 0.5 g L^{-1}) and particle size (G4): the kinetic rate, k_2, for the PSORE was of the same order of magnitude, i.e., 0.72×10^{-3} and 0.67×10^{-3} g mg^{-1} min^{-1} at pH 4 and pH 5, respectively; while the sorption capacity slightly increases with pH.

Again the comparison of q_m for model and experimental data shows a very good correlation when using the PFORE model. The kinetic parameter k_1 drastically reduces when increasing particle size; k_1 linearly decreases with the reciprocal of average diameter of particles, according to:

$$k_1 = 15.41 \times \left(\frac{1}{d}\right) + 0.020 \quad (R^2 = 0.997) \tag{4}$$

The kinetic parameter k_1 is very close at pH 4 and pH 5 for similar experimental conditions (Tables 1–2, G4 particle size and SD: 0.5 g L^{-1}). The variation of the kinetic parameters (both k_1 and k_2) with the reciprocal of the average diameter of sorbent particles is a first indication that the external surface plays a part in the control of uptake kinetics.

3.5. Effect of metal concentration (C_0)

Fig. 4 shows the effect of metal concentration on uptake kinetics at pH 5. Selected experimental conditions cover operating conditions: the highest concentration (i.e., 100 mg Pb L^{-1}) corresponds to the quasi-saturation of the sorbent, while the lowest concentration may correspond to a sorption limited to external layers. The equilibrium sorption capacity obviously increased with metal concentration (Table 3). The variation in the kinetic parameters are not high enough (in this concentration range) to define a clear trend. In the case of the PFORE model a good correlation was found between experimental and modeled values of q_m. The kinetic parameter slightly increased with the concentration (between 0.05 and 0.071 min^{-1} when increasing metal concentration from 20 to 100 mg Pb L^{-1}).

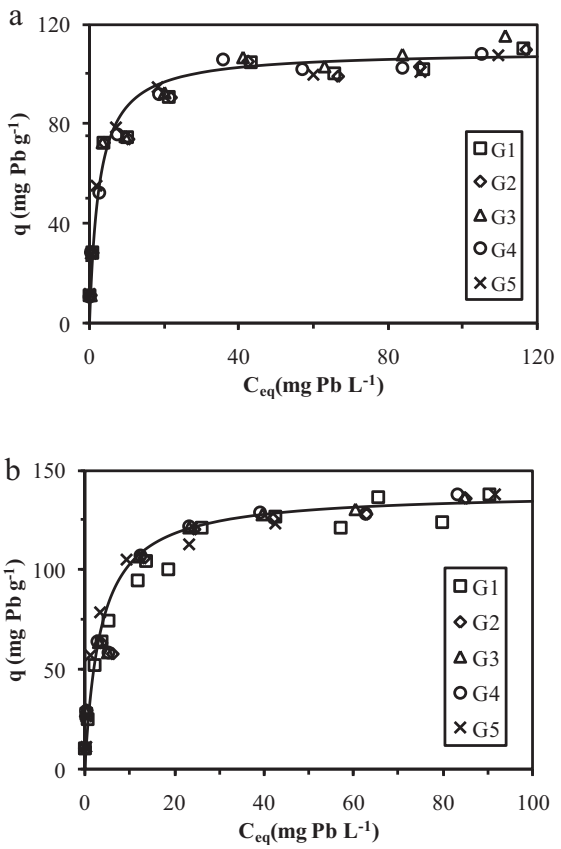

Fig. 5. Pb(II) sorption isotherms using *Posidonia* biosorbent—effect of initial pH: (a) pH 4, and (b) pH 5 (solid line represents the modeling of experimental data with the Langmuir equation and the parameters reported in Table 4 for combined data, joining all PS series).

The kinetic rate, k_2, decreased between 20 and 50 mg Pb L^{-1} but remained constant between 50 and 100 mg L^{-1}. In the case of methylene blue biosorption on *P. oceanica*, Ncibi et al. [44] observed a progressive increase of the kinetic rate for the PSORE with increasing metal concentration (between 10 and 40 mg dye L^{-1}) while at 50 mg dye L^{-1} the kinetic rate substantially decreased. In the case of Cr(VI) sorption on the same material the kinetic rate continuously increased with metal concentration [41]. A contrary trend was cited by Guezguez et al. [38] for the sorption of Yellow 59 dye on *P. oceanica*: the rate parameter decreased with increasing dye concentration.

3.6. Sorption isotherms

The sorption isotherms were obtained at initial pH 4 and 5 (Fig. 5) for different particle sizes (G1–G5). The experimental data were superimposed: this result confirms previous conclusion on the impact of particle size on uptake kinetics (Fig. 3 and Table 2). This means that all the reactive groups remain available for metal binding. A slight increase in the affinity coefficient was observed when increasing the size of sorbent particles. The different series were merged and the Langmuir equation was applied to cumulative data: the parameters are reported in Table 4.

The maximum sorption capacity reached 109 mg Pb g^{-1} (0.53 mmol Pb g^{-1}) at pH 4 and increased up to 140 mg Pb g^{-1} (0.68 mmol Pb g^{-1}) at pH 5. This increase in sorption capacity is consistent with the conclusions on pH effect (Fig. 1). The affinity coefficient (b coefficient) was close to 0.39 L mg^{-1} at pH 4 but slightly decreased to 0.3 L mg^{-1} at pH 5. Increasing the pH

Table 4
Sorption isotherms—parameters of the Langmuir equation.

pH	PS	Langmuir parameters		
		q_m (mg Pb g^{-1})	b (L mg^{-1})	R^2
4	G1	109.0	0.343	0.997
	G2	108.9	0.329	0.997
	G3	114.4	0.314	0.996
	G4	107.6	0.486	0.998
	G5	106.1	0.531	0.998
	Combined	109.1	0.388	0.996
5	G1	138.1	0.247	0.986
	G2	139.6	0.248	0.994
	G3	139.9	0.296	0.996
	G4	139.6	0.304	0.995
	G5	138.5	0.386	0.997
	Combined	138.8	0.283	0.992

Combined: modeling of sorption isotherms cumulating all the series (independently of particle size).

increased maximum sorption at the expense of a slight decrease of affinity coefficient.

These values are compared to the sorption performance of a series of alternative biosorbents in Table 5. Among the most efficient biosorbents are alginate-based materials, Ca-alginate and Na-alginate, with sorption capacities as high as 551 and 443 mg Pb g^{-1} [23]. Sorption capacities in the range 200–300 mg Pb g^{-1} were obtained using algae such as *Fucus vesiculosus* [17], *Chondracanthus chamissoi* [45] or *Sargassum natans* [46]. *P. oceanica* shows intermediary maximum sorption capacity with values of 109 and 140 mg Pb g^{-1}. This is comparable to the levels reached for *Oedogonium* sp. and *Nostoc* sp. [16] or *Streptomyces rimosus* [13], and much better than chitosan [25] or fungi such as *Rhizopus arrhizus* [47,48]. It is noteworthy that the affinity coefficient (b) was significantly higher for *P. oceanica* compared to other biosorbents (Table 5). *P. oceanica* was also tested for Cu(II) binding at pH 5 and 6 with sorption capacities close to 57 and 86 mg Cu g^{-1}, respectively (i.e., 0.9 and 1.35 mmol Cu g^{-1}) [40]. The affinity coefficients for Cu(II) were significantly lower than those of Pb(II): 6.35 and 8.26 L mmol^{-1} for Cu(II) (at pH 5 and 6, respectively) versus 62.8 and 80.4 L mmol^{-1} for Pb(II) (at pH 4 and 5, respectively). In the case of ammonium sorption using the same type of biosorbent, Wahab et al. [39] obtained very low sorption capacities (below 3 mg NH_4^+ g^{-1}) with affinity coefficients in the range 0.13–0.17 L mg^{-1}. In the case of Yellow 59 dye sorption on *P. oceanica*, Guezguez et al. [38] found sorption capacities close to 77 mg dye g^{-1} with very high affinity coefficient (close to 2.9 L mg^{-1}). For methylene blue sorption on *P. oceanica*, much lower Langmuir parameters were obtained (q_m: 5.6 mg dye g^{-1}, and b: 0.22 L mg^{-1}) [44].

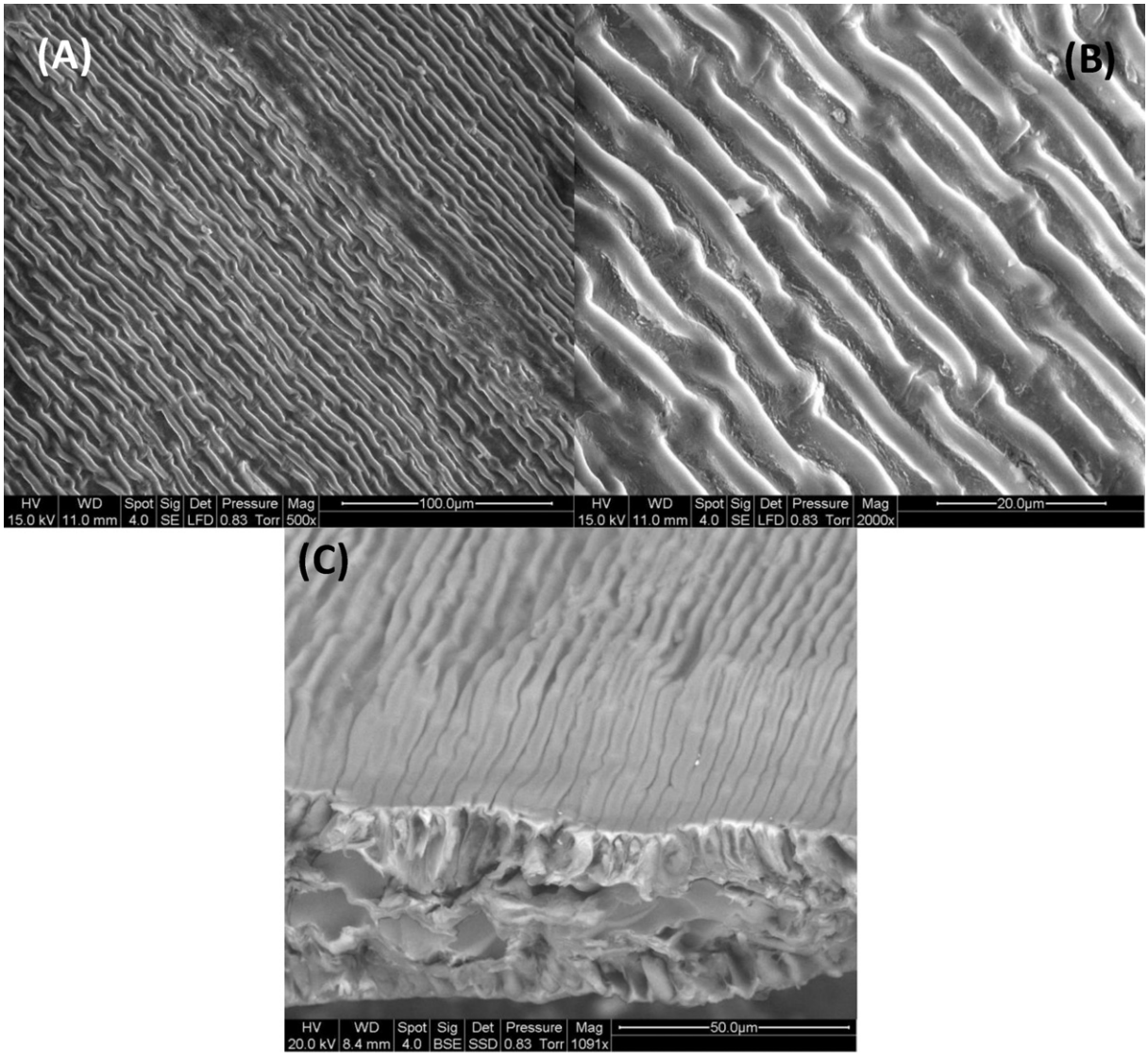

Fig. 6. SEM photographs of *Posidonia* biomass (scale bar: 100 µm (A), 50 µm (C), 20 µm (B)).

Table 5
Comparison of Pb(II) sorption for different biosorbents.

Biosorbent	pH	Specific experimental conditions	q_m or q_{max} (mg Pb g^{-1})	b (L mg^{-1})	Reference
Cereal chaff	5.5	20–30 °C	10–13	0.09–0.07	[21]
Chitosan beads	4.5	–	35	0.076	[25]
Na-alginate	6	30 °C	443	0.204	[23]
Ca-alginate	6	30 °C	551	0.023	[23]
Oedogonium sp.	5	25–45 °C	145–170	0.022–0.025	[16]
Nostoc sp.	5	25–45 °C	93–106	0.023–0.024	[16]
Phanaerochaete chrysosporium	4.5	27 °C	50*	–	[19]
Fucus vesiculosus	5	23 °C	211	0.06	[17]
Streptomyces rimosus	**	***	137	0.172	[13]
Cephalosporium aphidicola	5	20 °C	92	0.015	[20]
Pinus silvestris	4	25 °C	11	–	[49]
Zooglea ramigera	4.5	25 °C	10	–	[50]
Rhizopus arrhizus	5	25 °C	16	–	[50]
Rhizopus arrhizus	5–7	–	56	–	[51]
Sargassum natans	3.5	26 °C	310	–	[46]
Chondracanthus chamissoi	4–5	20 °C	280	0.089	[45]
Posidonia oceanica	4	20 °C	109	0.388	This study
Posidonia oceanica	5	20 °C	140	0.303	This study

* Incomplete isotherm (the saturation plateau was not reached).
** Unadjusted pH.
*** NaOH-treated biomass.

4. Material characterization

4.1. SEM and SEM-EDAX analyses

Scanning electron microscopy was used for characterizing the morphology and structure of the biosorbent. Fig. 6(A–B) shows the surface morphology of the biomass. This is a very-structured material characterized by a "fibrous" aspect. This is confirmed by Fig. 6(C) that shows the presence of lamellar structures on the external layers, while the central part of the ribbon-like material is characterized by a less-structured aspect. The surface morphology offers a more favorable area than a smooth-surface material; additionally,

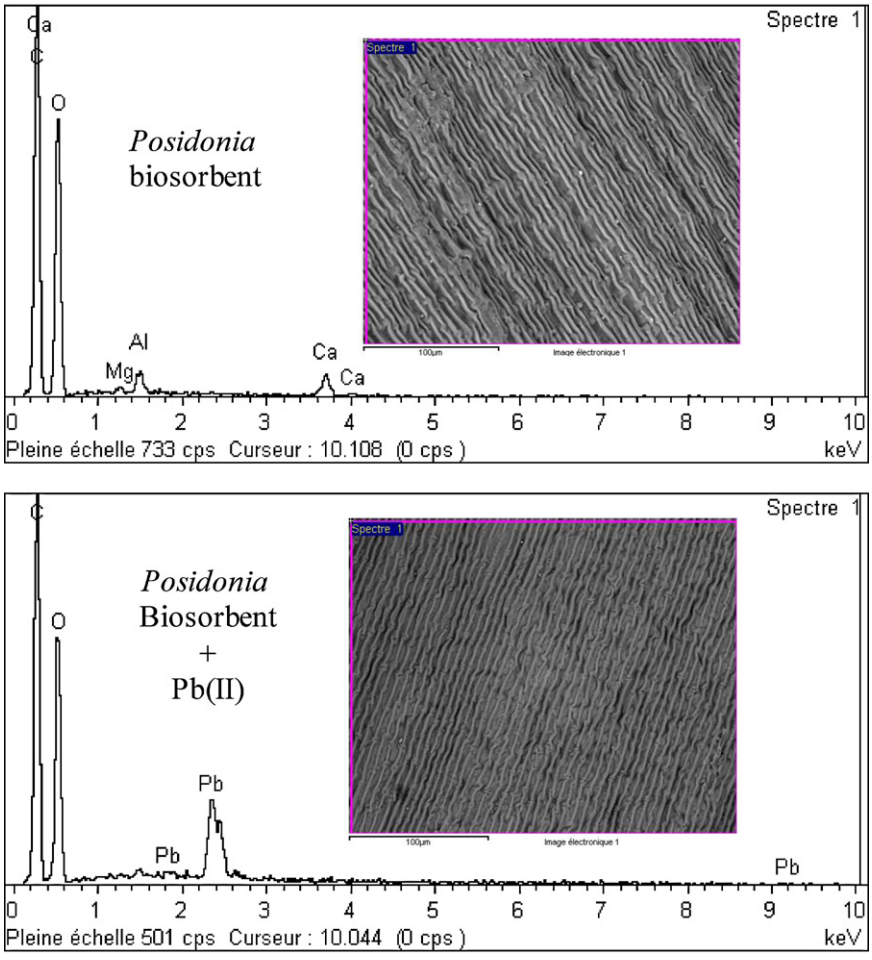

Fig. 7. SEM-EDAX analysis of *Posidonia* biosorbent before and after Pb(II) sorption.

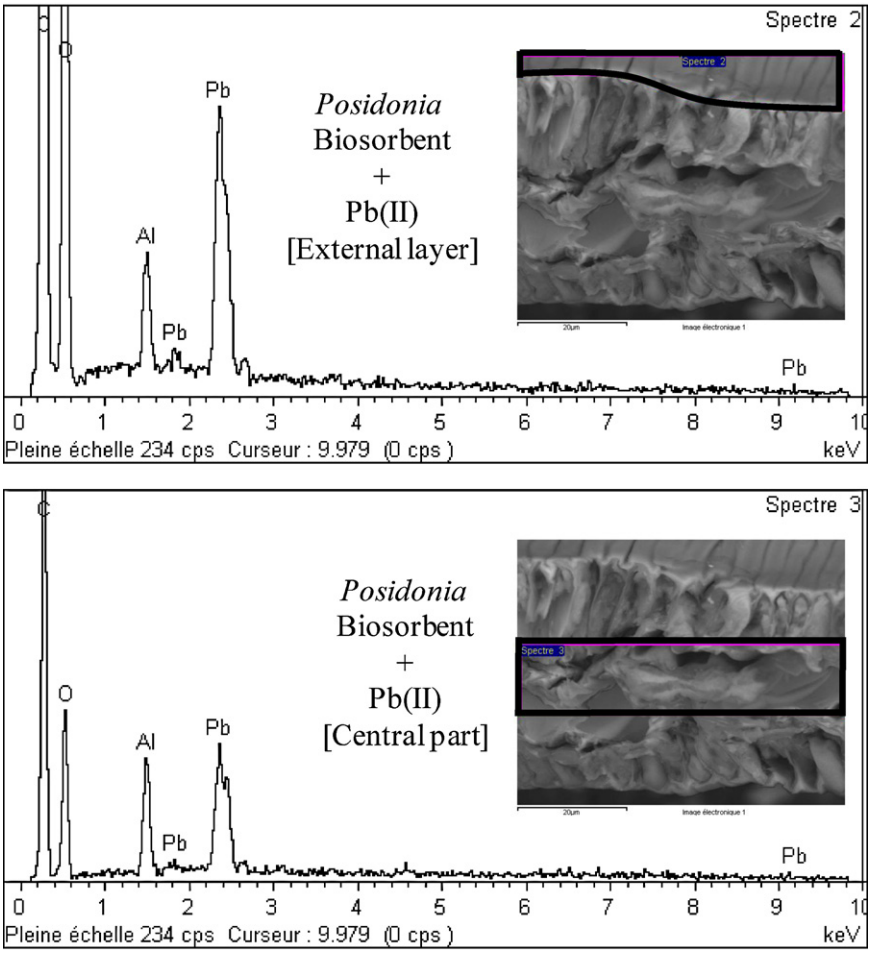

Fig. 8. SEM-EDAX analysis of *Posidonia* biosorbent after Pb(II) sorption—metal localization (framed zone corresponds to the surface area analyzed by EDAX).

the observation of the biosorbent section indicates that channels may exist in the external layers of the material that can make easier the diffusion of the solute to the center of the particles. This will be important for evaluating the contribution of the resistance to intraparticle diffusion on the control of uptake kinetics.

Fig. 7 shows the SEM-EDAX analyses of the biosorbent before and after Pb(II) sorption. The analyzed surface covers the whole external surface of the biomass shown on the SEM photographs. On the raw material the most representative elements (apart of carbon or oxygen) are Ca, Al and Mg. After Pb(II) sorption these elements

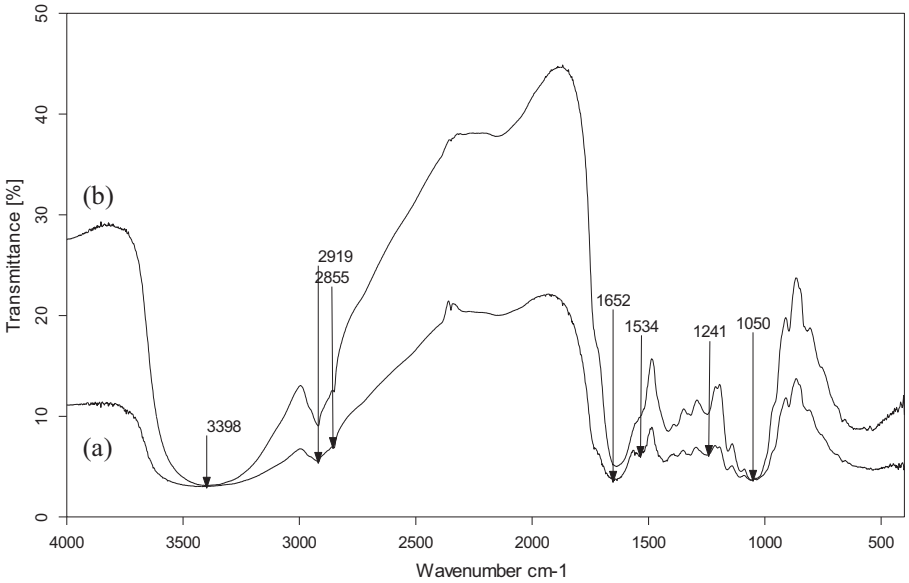

Fig. 9. FT-IR spectroscopy spectra for *Posidonia* biosorbent before (a) and after (b) Pb(II) sorption.

Table 6
XPS spectrometry analysis of biosorbent (raw and metal-loaded forms)—binding energies (BEs, eV) and atomic fraction (AF, %) of most significant elements.

		C_{1S}	N_{1S}	O_{1S}	$Pb_{4f_{7/2}}$
Raw *P. oceanica*	BEs (eV)	284.80 286.79 288.23	400.1	532.1	–
	AF (%)	73.4–74.6	4.85–4.44	20.56–17.49	–
P. oceanica + Pb(II)	BEs (eV)	284.78 286.49 288.13	400.1	532.1	138.7
	AF (%)	73.6–75.2	4.69–3.93	20.17–16.69	1.07–1.09

disappeared and they are replaced by Pb(II). This could indicate that metal binding occurs through ion exchange between divalent cations (Ca(II) and Mg(II)) and Pb(II). The phase-contrast photograph of Pb(II)-loaded biosorbent (not shown) does not indicate the presence of metal aggregates at the surface of the material. This means that the metal is probably bound uniformly at the surface of the biosorbent without occurrence of micro-precipitation. Fig. 8 compares the distribution of lead in cross-section of the biosorbent (the biosorbent was cut after metal sorption) showing the element analyses of the external layer and the central part of the biomass. Actually, the analytical probe detects the elements in a volumetric zone which is not limited to the surface: the analysis operates on peripheral layers. For this reason it is difficult to definitively conclude. However, the SEM-EDAX analysis shows that the amount of Pb is higher in the external layers than in the central part of the biosorbent. The difference in Pb concentration may indicate (a) diffusion limitations, (b) incomplete saturation of the biomass. In any case the metal can access the reactive groups located at the center of the biosorbent. It is also important to observe that Al element is present in much higher quantity than at the surface of the biomass (Figs. 7 and 8).

4.2. FT-IR spectroscopy analysis

The major components of *Posidonia* biomass are lignin, hemicellulose, and cellulose. Lignin is characterized by the presence of phenolic hydroxyl, aliphatic hydroxyl, methoxyl and carbonyl functional groups. Hemicellulose is constituted of different heteropolysaccharides (xylose, mannose, galactose...) associated on a disorganized (non-linear, ramified) mode with other polysaccharides and with lignin. Cellulose is characterized by a linear structure made of $\beta(1 \rightarrow 4)$ linked D-glucose units associated to other chains through hydrogen bonds; it is also rich in hydroxyl groups. FT-IR spectra for *P. oceanica* were recorded before and after Pb(II) biosorption (Fig. 9). The first part of the spectra (in the range 4000–2000 cm^{-1}) is poorly resolved: (a) a broad band is observed in the range 3700–3000 cm^{-1}, which is representative of the convolution of the signals for different vibration modes such as free OH, O–H stretch, and inter-chains H-bonds, (b) and two small peaks at 2919 cm^{-1} and 2855 cm^{-1} that correspond to symmetric $-CH_2$ valence vibration and –CH stretching vibration, respectively [52]. It is generally difficult finding useful information from this wavenumber range and spectrum analysis is generally focused on the 2000–600 cm^{-1} region. A band is observed close to 1652 cm^{-1}: this band is attributed to C=O stretch in conjugated p-substituted aryl ketones [52]. On this broad band, a shoulder can be observed at 1728 cm^{-1}: this is representative of either C=O stretch in unconjugated ketones, carbonyls and in ester groups (especially in carbohydrates) conjugated aldehydes and carboxylic acids, or C=O valence vibration of acetyl or COOH groups. The peak at 1534 cm^{-1} can be identified in amine/amide groups and in carboxyl groups. A series of peaks are identified in the range 1430–1300 cm^{-1}; they are non-specific bands that can be readily identified in cellulose material (1423, 1371, 1314 cm^{-1}) because the biopolymer is more crystalline than other constituents of hemicelluloses and lignin [53]. Another broad band appears at 1241 cm^{-1} that was attributed to symmetric stretching in carboxyl groups. The broad band around 1100 cm^{-1} (with a series of small peaks) is representative of carbohydrate ring bonds. The peak at 891 cm^{-1} can be probably attributed to anomere C-groups and ring valence vibration [52].

After Pb(II) binding, the spectrum is not drastically modified. The main differences can be observed (a) in the range 1750–1600 cm^{-1} where the width of the broad band is reduced (sharper and more resolved peak), at (b) 1534 cm^{-1} where the shoulder was less marked, and (c) at 1423 cm^{-1} and 1371 cm^{-1}, where the peaks slightly decreased. This probably means that some amine/amide groups may be involved together with cellulose functional groups. The band representative of the aromatic skeletal vibration of the phenol and phenolate in lignin are supposed to appear around 1512–1495 cm^{-1} (respectively) [54]. They may contribute in the change of the bands in this wavenumber range after metal sorption through the probable contribution of phenolic compounds.

4.3. XPS analysis

XPS spectrometry can be used for both quantifying the elements present on the sorbent (and their relative variation during the sorption process) and identifying their binding energy (that can be affected by the sorption process). The biosorbent was analyzed by XPS before and after metal binding (with experimental conditions corresponding to pH 5, SD: 0.5 $g\,L^{-1}$ and C_0: 100 mg Pb L^{-1}; this means a sorption capacity close to 140 mg Pb g^{-1}). Table 6 reports the BEs and the atomic fraction of the most significant elements. Actually, the sorption of lead had a negligible effect on the values of both BEs and atomic fractions.

5. Conclusion

P. oceanica is very efficient for Pb(II) biosorption. The interpretation of pH effect confirms that the binding of metal cations is favored at near neutral pH, probably through electrostatic binding on anionic groups (after deprotonation of surface reactive groups) or ion exchange with alkaline and alkaline-earth elements (as shown by SEM-EDAX). The optimum pH is found close to pH 4–5. The asymptotic trend of the sorption isotherm confirms that the equilibrium is preferentially described by the Langmuir equation (rather than the Freundlich equation). Maximum sorption capacities reach 109 mg Pb g^{-1} (at pH 4) and 140 mg Pb g^{-1} (at pH 5). The affinity coefficient is in the range 0.3–0.38 L mg^{-1}; this means ones of the highest among conventional biosorbents. The particle size does not affect sorption capacity at equilibrium indicating that all reactive groups remain accessible. This is consistent with the SEM-EDAX observations that show the presence of lead at the center of biosorbent particles. Additionally, the particle size hardly changes the uptake profiles: this means that the intraparticle diffusion is probably not the predominant controlling step in the sorption process. This is consistent with the observation of biosorbent structure

through SEM analysis: the lamellar structure of the biosorbent (at the surface) enhances the accessibility of solute to the center of the particles. Uptake profiles were better fitted by the pseudo-first order rate equation (PFORE) than by the pseudo-second order rate equation (PSORE). The kinetic parameter (k_1 for PFORE) linearly increases with sorbent dosage and linearly decreased with the reciprocal of the average diameter of sorbent particles, while the concentration has a limited impact on kinetic parameter.

Nomenclature

b	Langmuir constant ($L\,mg^{-1}$)
C_0	initial concentration of metal in solution (mg/L^{-1})
C_{eq}	equilibrium concentration of metal in solution ($mg\,L^{-1}$)
D	average particle diameter for selected particle size sample (μm)
D_{eff}	effective diffusivity ($m^2\,min^{-1}$)
k_1	rate constant of first-order kinetic model (min^{-1})
k_2	rate constant of pseudo-second-order kinetic model ($g\,mg^{-1}\,min^{-1}$)
m	mass of biomass (g)
q	adsorbed metal ion quantity per gram of biomass at any time ($mg\,g^{-1}$)
q_{eq}	adsorbed metal ion quantity per gram of biomass at equilibrium ($mg\,g^{-1}$)
q_m	maximum amount of adsorbed metal per gram of biomass ($mg\,g^{-1}$)
q_{mod}	modeled equilibrium sorption capacity ($mg\,g^{-1}$)
R^2	correlation coefficient
t	time (min)
V	solution volume (L)

Acknowledgements

N.A. acknowledges the financial support of Grant PNE (Programme National Exceptionnel, Algeria) for the fellowship at EMA. Authors thank J.-M. Taulemesse and R. Lorquet (from Centre des Matériaux de Grande Diffusion, Ecole des Mines d'Alès) for SEM/SEM-EDAX and FT-IR spectroscopy analyses, respectively. Prof. Enrique Rodriguez Castellon from Universidad de Malaga (Spain) is acknowledged for performing XPS analysis.

Appendix A. Supplementary data

Supplementary data associated with this article can be found, in the online version, at doi:10.1016/j.cej.2011.02.005.

References

[1] European Union, Council Directive 98/83/EC of 3rd November 1998 on the quality of water intended for human consumption, in: Official Journal of the European Community, Brussels, Belgium, 1998, pp. L330/332–L330/354.

[2] I. Komjarova, R. Blust, Comparison of liquid–liquid extraction, solid-phase extraction and co-precipitation preconcentration methods for the determination of cadmium, copper, nickel, lead and zinc in seawater, Anal. Chim. Acta 576 (2006) 221–228.

[3] A. Oliva, A. Molinari, F. Zuniga, P. Ponce, Studies on the liquid–liquid extraction of nickel(II), zinc(II), cadmium(II), mercury(II) and lead(II) with 1-phenyl-3-hydroxy-4-dodecyldithiocarboxylate-5-pyrazolone, Microchim. Acta 140 (2002) 201–203.

[4] K. Fujinaga, H. Nagura, R. Yamasaki, H. Kokusen, Y. Komatsu, Y. Seike, M. Okumura, The selective liquid–liquid extraction of cadmium(II) and lead(II) with 2-pyridinealdoxime, Solvent Extr. Res. Dev. Jpn. 13 (2006) 175–184.

[5] N.A. Badawy, A.A. El-Bayaa, A.Y. Abdel-Aal, S.E. Garamon, Chromatographic separations and recovery of lead ions from a synthetic binary mixtures of some heavy metal using cation exchange resin, J. Hazard. Mater. 166 (2009) 1266–1271.

[6] M.V. Dinu, E.S. Dragan, A.W. Trochimczuk, Sorption of Pb(II), Cd(II) and Zn(II) by iminodiacetate chelating resins in non-competitive and competitive conditions, Desalination 249 (2009) 374–379.

[7] L. Dong, Z. Zhu, H. Ma, Y. Qiu, J. Zhao, Simultaneous adsorption of lead and cadmium on MnO_2-loaded resin, J. Environ. Sci. 22 (2010) 225–229.

[8] C. Xiong, C. Yao, Synthesis, characterization and application of triethylenetetramine modified polystyrene resin in removal of mercury, cadmium and lead from aqueous solutions, Chem. Eng. J. 155 (2009) 844–850.

[9] B. Mandal, N. Ghosh, Extraction chromatographic method of preconcentration and separation of lead (II) with high molecular mass liquid cation exchanger, Desalination 250 (2010) 506–514.

[10] R.-S. Juang, S.-W. Wang, L.-C. Lin, Simultaneous recovery of EDTA and lead(II) from their chelated solutions using a cation exchange membrane, J. Membr. Sci. 160 (1999) 225–233.

[11] O. Kebiche-Senhadji, L. Mansouri, S. Tingry, P. Seta, M. Benamor, Facilitated Cd(II) transport across CTA polymer inclusion membrane using anion (Aliquat 336) and cation (D2EHPA) metal carriers, J. Membr. Sci. 310 (2008) 438–445.

[12] M.A. Dubois, J.F. Dozol, C. Nicotra, J. Serose, C. Massiani, Pyrolysis and incineration of cationic and anionic ion-exchange resins—identification of volatile degradation compounds, J. Anal. Appl. Pyrol. 31 (1995) 129–140.

[13] A. Selatnia, A. Boukazoula, N. Kechid, M.Z. Bakhti, A. Chergui, Y. Kerchich, Biosorption of lead (II) from aqueous solution by a bacterial dead *Streptomyces rimosus* biomass, Biochem. Eng. J. 19 (2004) 127–135.

[14] K. Vijayaraghavan, Y.S. Yun, Bacterial biosorbents and biosorption, Biotechnol. Adv. 26 (2008) 266–291.

[15] O.M.M. Freitas, R.J.E. Martins, C.M. Delerue-Matos, R.A.R. Boaventura, Removal of Cd(II), Zn(II) and Pb(II) from aqueous solutions by brown marine macro algae: kinetic modelling, J. Hazard. Mater. 153 (2008) 493–501.

[16] V.K. Gupta, A. Rastogi, Biosorption of lead(II) from aqueous solutions by non-living algal biomass *Oedogonium* sp. and *Nostoc* sp.—a comparative study, Colloids Surf., B 64 (2008) 170–178.

[17] Y.N. Mata, M.L. Blázquez, A. Ballester, F. González, J.A. Muñoz, Characterization of the biosorption of cadmium, lead and copper with the brown alga *Fucus vesiculosus*, J. Hazard. Mater. 158 (2008) 316–323.

[18] J.L. Wang, C. Chen, Biosorption of heavy metals by *Saccharomyces cerevisiae*: a review, Biotechnol. Adv. 24 (2006) 427–451.

[19] Q. Li, S. Wu, G. Liu, X. Liao, X. Deng, D. Sun, Y. Hu, Y. Huang, Simultaneous biosorption of cadmium (II) and lead (II) ions by pretreated biomass of *Phanerochaete chrysosporium*, Sep. Purif. Technol. 34 (2004) 135–142.

[20] S. Tunali, T. Akar, A.S. Özcan, I. Kiran, A. Özcan, Equilibrium and kinetics of biosorption of lead(II) from aqueous solutions by *Cephalosporium aphidicola*, Sep. Purif. Technol. 47 (2006) 105–112.

[21] R. Han, J. Zhang, W. Zou, J. Shi, H. Liu, Equilibrium biosorption isotherm for lead ion on chaff, J. Hazard. Mater. 125 (2005) 266–271.

[22] A. Demirbas, Heavy metal adsorption onto agro-based waste materials: a review, J. Hazard. Mater. 157 (2008) 220–229.

[23] M. Khotimchenko, V. Kovalev, Y. Khotimchenko, Comparative equilibrium studies of sorption of Pb(II) ions by sodium and calcium alginate, J. Environ. Sci. 20 (2008) 827–831.

[24] V.V. Kobak, M.V. Sutkevich, I.G. Plashchina, E.E. Braudo, Non-stoichiometric binding of lead(II) ions by sodium alginate, J. Inorg. Biochem. 61 (1996) 221–226.

[25] W.S.W. Ngah, S. Fatinathan, Pb(II) biosorption using chitosan and chitosan derivatives beads: equilibrium, ion exchange and mechanism studies, J. Environ. Sci. 22 (2010) 338–346.

[26] B. Volesky, Sorption and Biosorption, BV Sorbex, Inc., Montréal, St. Lambert, Québec, Canada, 2003.

[27] E. Romera, F. Gonzalez, A. Ballester, M.L. Blazquez, J.A. Munoz, Biosorption with algae: a statistical review, Crit. Rev. Biotechnol. 26 (2006) 223–235.

[28] R. Khiari, M.F. Mhenni, M.N. Belgacem, E. Mauret, Chemical composition and pulping of date palm rachis and *Posidonia oceanica*—a comparison with other wood and non-wood fibre sources, Bioresour. Technol. 101 (2010) 775–780.

[29] C. Lafabrie, C. Pergent-Martini, G. Pergent, Metal contamination of *Posidonia oceanica* meadows along the Corsican coastline (Mediterranean), Environ. Pollut. 151 (2008) 262–268.

[30] C. Lafabrie, G. Pergent, C. Pergent-Martini, A. Capiomont, *Posidonia oceanica*: a tracer of past mercury contamination, Environ. Pollut. 148 (2007) 688–692.

[31] G. Pergent, C. Pergent-Martini, Mercury levels and fluxes in *Posidonia oceanica* meadows, Environ. Pollut. 106 (1999) 33–37.

[32] M. Warnau, G. Ledent, A. Temara, J.-M. Bouquegneau, M. Jangoux, P. Dubois, Heavy metals in *Posidonia oceanica* and *Paracentrotus lividus* from seagrass beds of the north-western Mediterranean, Sci. Total Environ. 171 (1995) 95–99.

[33] M.C. Ncibi, B. Mahjoub, M. Seffen, Biosorption of phenol onto *Posidonia oceanica* (L.) seagrass in batch system: equilibrium and kinetic modelling, Can. J. Chem. Eng. 84 (2006) 495–500.

[34] M.C. Ncibi, B. Mahjoub, A.M.B. Hamissa, R.B. Mansour, M. Seffen, Biosorption of textile metal-complexed dye from aqueous medium using *Posidonia oceanica* (L.) leaf sheaths: mathematical modelling, Desalination 243 (2009) 109–121.

[35] M.C. Ncibi, B. Mahjoub, M. Seffen, Adsorption of metal dye by the fibres of *Posidonia oceanica*, J. Environ. Eng. Sci. 7 (2008) 645–650.

[36] M.C. Ncibi, B. Mahjoub, M. Seffen, Investigation of the sorption mechanisms of metal-complexed dye onto *Posidonia oceanica* (L.) fibres through kinetic modelling analysis, Bioresour. Technol. 99 (2008) 5582–5589.

[37] M.C. Ncibi, B. Mahjoub, M. Seffen, Adsorptive removal of textile reactive dye using *Posidonia oceanica* (L.) fibrous biomass, Int. J. Environ. Sci. Technol. 4 (2007) 433–440.

[38] I. Guezguez, S. Dridi-Dhaouadi, F. Mhenni, Sorption of Yellow 59 on *Posidonia oceanica*, a non-conventional biosorbent: comparison with activated carbons, Ind. Crops Prod. 29 (2009) 197–204.

[39] M.A. Wahab, S. Jellali, N. Jedidi, Effect of temperature and pH on the biosorption of ammonium onto *Posidonia oceanica* fibers: equilibrium, and kinetic modeling studies, Bioresour. Technol. 101 (2010) 8606–8615.
[40] M. Izquierdo, C. Gabaldón, P. Marzal, F.J. Álvarez-Hornos, Modeling of copper fixed-bed biosorption from wastewater by *Posidonia oceanica*, Bioresour. Technol. 101 (2010) 510–517.
[41] M.C. Ncibi, B. Mahjoub, M. Seffen, F. Brouers, S. Gaspard, Sorption dynamic investigation of chromium(VI) onto *Posidonia oceanica* fibres: kinetic modelling using new generalized fractal equation, Biochem. Eng. J. 46 (2009) 141–146.
[42] A. Chadlia, K. Mohamed, L. Najah, M.h.M. Farouk, Preparation and characterization of new succinic anhydride grafted *Posidonia* for the removal of organic and inorganic pollutants, J. Hazard. Mater. 172 (2009) 1579–1590.
[43] G. Ledent, M.A. Mateo, M. Warnau, A. Temara, J. Romero, P. Dubois, Element losses following distilled water rinsing of leaves of the seagrass *Posidonia oceanica* (L.) *Delile*, Aquat. Bot. 52 (1995) 229–235.
[44] M.C. Ncibi, B. Mahjoub, M. Seffen, Kinetic and equilibrium studies of methylene blue biosorption by *Posidonia oceanica* (L.) fibres, J. Hazard. Mater. 139 (2007) 280–285.
[45] A. Yipmantin, H.J. Maldonado, M. Ly, J.-M. Taulemesse, E. Guibal, Pb(II) and Cd(II) biosorption on *Chondracanthus chamissoi* (a red alga), J. Hazard. Mater. 185 (2011) 922–929.
[46] Z.R. Holan, B. Volesky, Biosorption of Lead and Nickel by Biomass of Marine Algae, Wiley Subscription Services, Inc., A Wiley Company, 1994, pp. 1001–1009.
[47] Y. Sag, T. Kutsal, The simultaneous biosorption process of lead(II) and nickel(II) on *Rhizopus arrhizus*, Process Biochem. 32 (1997) 591–597.
[48] Y. Sag, T. Kutsal, Determination of the biosorption activation energies of heavy metal ions on *Zoogloea ramigera* and *Rhizopus arrhizus*, Process Biochem. 35 (2000) 801–807.
[49] H. Ucun, Y.K. Bayhana, Y. Kaya, A. Cakici, O.F. Algur, Biosorption of lead (II) from aqueous solution by cone biomass of *Pinus sylvestris*, Desalination 154 (2003) 233–238.
[50] Y. Sag, D. Özer, T. Kutsal, A comparative study of the biosorption of lead(II) ions to *Z. ramigera* and *R. arrhizus*, Process Biochem. 30 (1995) 169–174.
[51] E. Fourest, J.-C. Roux, Heavy metal biosorption by fungal mycelial by-products: mechanisms and influence of pH, Appl. Microbiol. Biotechnol. 37 (1992) 399–403.
[52] M. Schwanninger, J.C. Rodrigues, H. Pereira, B. Hinterstoisser, Effects of short-time vibratory ball milling on the shape of FT-IR spectra of wood and cellulose, Vibrational Spectrosc. 36 (2004) 23–40.
[53] M. Åkerholm, L. Salmén, Interactions between wood polymers studied by dynamic FT-IR spectroscopy, Polymer 42 (2001) 963–969.
[54] P. Käuper, D. Ferri, From production to product: part 2, FT-IR spectroscopy as a tool for quality control in the preparation of alkaline solutions of bagasse lignin, Ind. Crops Prod. 20 (2004) 159–167.